



## Synthesis and radiopharmacological investigation of 3-[4'-<sup>18</sup>F]fluorobenzylidene]indolin-2-one as possible tyrosine kinase inhibitor

Torsten Knies <sup>a,\*</sup>, Ralf Bergmann <sup>a</sup>, Manuela Kuchar <sup>a</sup>, Jörg Steinbach <sup>a</sup>, Frank Wuest <sup>b</sup>

<sup>a</sup>Institute of Radiopharmacy, Forschungszentrum Dresden-Rossendorf e.V., PO Box 510119, D-01314 Dresden, Germany

<sup>b</sup>Department of Oncologic Imaging, Cross Cancer Institute, University of Alberta, Edmonton, Alberta, Canada T6G 1Z2

### ARTICLE INFO

#### Article history:

Received 12 June 2009

Revised 15 September 2009

Accepted 21 September 2009

Available online 25 September 2009

#### Keywords:

Positron emission tomography (PET)

4-[<sup>18</sup>F]fluorobenzaldehyde

Tyrosine kinase inhibitor

Knoevenagel condensation

SU5416

### ABSTRACT

The radiosynthesis and radiopharmacological evaluation of 3-[4'-<sup>18</sup>F]fluorobenzylidene]indolin-2-one, a derivative of tyrosine kinase inhibitor SU5416, is described. The radiosynthesis was accomplished by Knoevenagel condensation of 4-[<sup>18</sup>F]fluorobenzaldehyde with oxindole in a remotely controlled synthesis module. The reaction conditions were optimized through screening the influence of different bases on the radiochemical yield. The radiotracer was obtained after a two-step labelling procedure in 4% decay-corrected radiochemical yield at a specific activity of 48–61 GBq/μmol within 90 min. The radiochemical purity after semi-preparative HPLC purification exceeded 98%.

The biodistribution was studied in Wistar rats. After distribution the radiotracer was rapidly accumulated in the adrenals, liver and kidneys, however, it was cleared from these and the most other organs. Only the adipose tissue remained the activity over 60 min. Unexpected high transient uptake was observed in the brain, pancreas, heart and lung. The fast clearance of 3-[4'-<sup>18</sup>F]fluorobenzylidene]indolin-2-one was caused by excretion, approximately one half each was renal and biliary excreted and the other part cleared by metabolic processes. In arterial blood plasma two more polar metabolites were found by radio-HPLC. After 20 min post-injection, only 12% of intact radiotracer has been detected. Consequently, in small animal PET studies with FaDu tumour bearing mice no specific uptake in the tumours could be observed.

© 2009 Elsevier Ltd. All rights reserved.

### 1. Introduction

Receptor tyrosine kinases (RTKs) are membrane-spanning cell surface proteins positioned in key crossroads within the cellular communication network. As master switches, RTKs play critical roles in the transduction of extracellular signals to the cytoplasm.<sup>1</sup> Moreover, RTKs have been found to play an important role in tumour angiogenesis through signal regulation for proliferation, migration and differentiation between tumour and endothelial cells.<sup>2</sup> Activated forms of these enzymes can result in enhanced tumour cell proliferation and growth, induction of anti-apoptotic effects, and angiogenesis and metastasis.<sup>3</sup> Many human cancers derive from epithelial tissues, and RTKs are often over-expressed in these tumours. This finding led to the development of several selective tyrosine kinase inhibitors with potencies in the nano- and subnanomolar range. Small molecule tyrosine kinase inhibitors like Imatinib mesylate (Gleevec<sup>®</sup>), Gefitinib (Iressa<sup>®</sup>), Erlotinib (Tarceva<sup>®</sup>), Vatalinib<sup>®</sup> (PTK 787) and Sorafinib<sup>®</sup> (BAY43-9006) as

potent anti-cancer agents have been approved or are currently studied in clinical trials.<sup>3,4</sup>

The growing number of anti-angiogenic therapies is accompanied with an increasing need for imaging tumour neovascularization, and monitoring anti-angiogenic therapies. Positron emission tomography (PET) is a powerful *in vivo* diagnostic molecular imaging technique applying tracer concentrations in the picomolar range to allow visualization of specific targets on the molecular level.<sup>5,6</sup> Direct noninvasive molecular imaging of angiogenesis would allow patient selection for anti-angiogenesis therapy, and assessment of the efficacy of angiogenesis targeted therapies.<sup>6</sup> Overexpression of tyrosine kinases in various human cancers represents an attractive basis for the development of small molecule tyrosine kinase inhibitors labelled with the short-lived positron emitters carbon-11 (<sup>11</sup>C, *t*<sub>1/2</sub> = 20.4 min) and fluorine-18 (<sup>18</sup>F, *t*<sub>1/2</sub> = 109.8 min) as molecular probes for imaging RTK expression *in vivo*. Recently, anilinoquinazoline-based tyrosine kinase inhibitor gefitinib (Iressa<sup>®</sup>) was used as a lead structure for the development of various <sup>11</sup>C-labelled<sup>7–11</sup> and <sup>18</sup>F-labelled radiotracers.<sup>12–15</sup> However, the majority of these reports describe mainly radiochemistry and *in vitro* experiments on inhibition of autophosphorylation. Only one report deals with the study of tumour uptake *in vivo* in xenografted tumour model rats involving a radiolabelled

\* Corresponding author. Tel.: +49 351 260 2760; fax: +49 351 260 2915.  
E-mail address: [t.kniess@fzd.de](mailto:t.kniess@fzd.de) (T. Knies).

tyrosine kinase inhibitor.<sup>11</sup> More recently, the synthesis and radiopharmacological evaluation of the <sup>11</sup>C-labelled tyrosine kinase inhibitor Gleevec<sup>®</sup> was studied by means of PET in baboons.<sup>16</sup>

Another class of small lipophilic RTK inhibitors are based on an oxindole scaffold. Prominent examples are SU5416 (Semaxinib<sup>®</sup>) and SU11248 (Sutent<sup>®</sup>), which have entered preclinical and multicenter clinical studies as inhibitors of vascular endothelial growth factor receptor (VEGFR) and for anti-angiogenic and antitumour activity<sup>3</sup> (Fig. 1).

SU11248 has been approved as anticancer agent for treatment of kidney cancer and gastrointestinal stromal tumours, whereas randomized phase III studies of SU5416 in patients with metastatic colorectal cancer failed for no showing survival benefits and revealing toxic side effects.<sup>17</sup> However, oxindole SU5416 exhibits high affinity towards VEGF-RTKs (IC<sub>50</sub> = 0.06 μM; <sup>18</sup> IC<sub>50</sub> < 0.8 μM<sup>24</sup>), and demonstrated anti-angiogenic activity in mice tumour xenografts.

Thus, compound SU5416 holds promise as molecular probe for imaging RTKs expression in tumour by means of PET. Synthesis of <sup>18</sup>F-labelled SU11248 starting from the corresponding nitro-precursor was recently described. However, no radiopharmacological data have been reported.<sup>19</sup>

The aim of the present study is the development of a general synthesis approach for the preparation of <sup>18</sup>F-labelled benzylidene oxindoles as potential radiotracers for PET imaging. The radiosynthesis of compounds containing the characteristic benzylidene oxindole scaffold as found in SU5416 was achieved via Knoevenagel condensation with the readily available <sup>18</sup>F labelling precursor 4-[<sup>18</sup>F]fluorobenzaldehyde. The novel radiotracer was used in radiopharmacological studies involving biodistribution in mice, metabolic stability assessment in vivo and small animal PET studies in FaDu tumour-bearing mice.

## 2. Materials and methods

### 2.1. Materials

All commercial reagents and solvents were used without further purification unless otherwise specified. Nuclear magnetic resonance spectra were recorded on a Varian Unity 400 MHz spectrometer. <sup>1</sup>H NMR chemical shifts were given in ppm and were referenced with the residual solvent resonances relative to tetramethylsilane (TMS). Mass spectra were obtained on a Quattro/LC mass spectrometer (MICROMASS) by electrospray ionization.

Flash chromatography was conducted using MERCK silica gel (mesh size 230–400 ASTM). Thin-layer chromatography (TLC) was performed on Merck silica gel F-254 aluminium plates with visualization under UV (254 nm).

No-carrier-added aqueous [<sup>18</sup>F]fluoride ion was produced in a IBA CYCLONE 18/9 cyclotron by irradiation of [<sup>18</sup>O]H<sub>2</sub>O via the <sup>18</sup>O(p,n)<sup>18</sup>F nuclear reaction. Synthesis of 4-[<sup>18</sup>F]fluorobenzaldehyde

and Knoevenagel condensation was performed in an automated nucleophilic fluorination module (Nuclear Interface, Münster, Germany). Semi-preparative HPLC purifications were carried out with a Nucleosil 100-7 C18 column (250 × 16 mm, 7 μm, Macherey-Nagel) using an isocratic eluent (acetonitrile/water = 1:1) with a flow rate of 8 mL/min. The product was monitored by UV detector UV2075 (Jasco) and by radioactivity detector integrated in the synthesizer module. Analytical HPLC analysis were carried out with a Discovery C18 column (15 × 4 mm, 5 μm, Suppelco) using an isocratic eluent (acetonitrile/water = 40:60) by a gradient pump L2500 (MERCK, HITACHI) with a flow rate of 1 mL/min. The products were monitored by an UV detector L4500 (MERCK, HITACHI) at 254 nm and by gamma-detection with a scintillation detector GABI (X-RAYTEST).

### 2.2. Synthesis of reference compounds and precursors

#### 2.2.1. 3-[(2,4'-Dimethylpyrrol-5'-yl)methylidene]5-fluoroindolin-2-one 2

Hundred and fifty milligrams (1 mmol) of 5-fluoro-oxindole 1 and 148 mg (1.2 mmol) of 3,5-dimethylpyrrol-2-carbaldehyde were refluxed in 2 mL of ethanol with 2 drops of piperidine for 4–5 h. The product was collected by filtration and purified by column chromatography (silica gel, ethyl acetate/petrol ether = 1:1). Yield: 79 mg orange crystals (31%), mp: 271–273 °C; <sup>1</sup>H NMR (δ, ppm, DMSO-*d*<sub>6</sub>): 2.30 (s, 3H, CH<sub>3</sub>); 2.32 (s, 3H, CH<sub>3</sub>); 6.02 (s, 1H, H<sub>pyrrol</sub>); 6.82 (d, 1H, 7-H); 6.88 (t, 1H, 6-H); 7.63 (s, 1H, H<sub>vinyl</sub>); 7.66 (d, 1H, 4-H); 10.77 (s, 1H, NH<sub>oxindole</sub>); ESI-MS (ES<sup>+</sup>): *m/z* = 257 (M+H).

#### 2.2.2. 3-[(2,4'-Dimethylpyrrol-5'-yl)methylidene]5-nitroindolin-2-one 5

The compound was prepared from 5-nitro-oxindole 3 and 3,5-dimethylpyrrol-2-carbaldehyde in 72% yield as previously described.<sup>20</sup>

#### 2.2.3. 3-[(2,4'-Dimethylpyrrol-5'-yl)methylidene]5-dimethylamino-indolin-2-one 6

Three hundred and fifty two milligrams (2 mmol) of 5-dimethylamino-oxindole 4<sup>21</sup> and 295 mg (2.4 mmol) of 3,5-dimethylpyrrol-2-carbaldehyde were refluxed in 4 mL of ethanol with 5 drops of piperidine for 6 h. The solvent was evaporated and the residue purified by column chromatography (silica gel, ethyl acetate/petrol ether = 1:1). Yield: 519 mg dark crystals (92%), mp: 260–267 °C, <sup>1</sup>H NMR (δ, ppm, DMSO-*d*<sub>6</sub>): 2.31 (2s, 6H, 2 × CH<sub>3</sub><sub>pyrrol</sub>); 2.86 (s, 6H, 2 × CH<sub>3</sub>); 5.97 (s, 1H, H<sub>pyrrol</sub>); 6.54 (d, 1H, 6-H); 6.70 (d, 1H, 7-H); 7.22 (s, 1H, 4-H); 7.55 (s, 1H, H<sub>vinyl</sub>); 10.45 (s, 1H, NH<sub>oxindole</sub>); ESI-MS (ES<sup>+</sup>): *m/z* = 282 (M+H).

#### 2.2.4. 5-Trimethylammonium-3-[(2,4'-dimethylpyrrol-5'-yl)methylidene]indolin-2-one-trifluoromethanesulfonate 7

Three hundred milligrams (1.06 mmol) of 6 were dissolved in 10 mL of dichloromethane and 140 μL (1.3 mmol) of ethyl-trifluoromethanesulfonate were added at rt. After stirring for 24 h the precipitate was collected by filtration and washed with 2 mL of dichloromethane. Yield: 360 mg brown precipitate (76%), mp: >280 °C, subl., <sup>1</sup>H NMR (δ, ppm, DMSO-*d*<sub>6</sub>): 2.35 (2s, 6H, 2 × CH<sub>3</sub><sub>pyrrol</sub>); 3.62 (s, 9H, 3 × CH<sub>3</sub>); 6.09 (s, 1H, H<sub>pyrrol</sub>); 7.00 (d, 1H, 7-H); 7.61 (d, 1H, 6-H); 7.77 (s, 1H, H<sub>vinyl</sub>); 8.28 (s, 1H, 4-H); 11.11 (s, 1H, NH<sub>oxindole</sub>); ESI-MS (ES<sup>+</sup>): *m/z* = 296 (M+).

#### 2.2.5. 3-[4'-Fluorobenzylidene]indolin-2-one 10 (SU5205)

The synthesis was carried out with 133 mg (1 mmol) oxindole and 129 μL (1.2 mmol) of 4-fluorobenzaldehyde following the procedure in 2.2.1., the product was purified by column chromatography (silica gel, trichloromethane/methanol 95:5). Yield: 103 mg

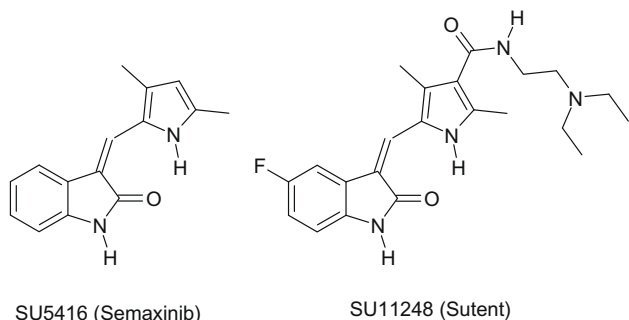


Figure 1. Structures of the tyrosine kinase inhibitors SU5416 and SU11248.

yellow crystals (43%), mp: 185–189 °C;  $^1\text{H}$  NMR ( $\delta$ , ppm, DMSO- $d_6$ ): 6.82 (m, 2H,  $\text{H}_{\text{oxindole}}$ ); 7.23 (t, 1H,  $\text{H}_{\text{oxindole}}$ ); 7.36 (m, 2H,  $\text{H}_{\text{benzyl}}$ ); 7.49 (d, 1H,  $\text{H}_{\text{oxindole}}$ ); 7.60 (s, 1H,  $\text{H}_{\text{vinyl}}$ ); 7.77 (d, 2H,  $\text{H}_{\text{benzyl}}$ ); 10.62 (s, 1H, NH); ESI-MS (ES+):  $m/z = 261$  (M+Na).

### 2.2.6. 3-[4'-Nitrobenzylidene]indoline-2-one 11

The synthesis was carried out using 133 mg (1 mmol) oxindole and 181 mg (1.2 mmol) of 4-nitrobenzaldehyde following the procedure in 2.2.1., the product was collected by filtration, and washed with 3 mL ethyl acetate. Yield: 217 mg yellow crystals (82%), mp: 245–250 °C;  $^1\text{H}$  NMR ( $\delta$ , ppm, DMSO- $d_6$ ): 6.84 (m, 2H,  $\text{H}_{\text{oxindole}}$ ); 7.26 (t, 1H,  $\text{H}_{\text{oxindole}}$ ); 7.40 (d, 1H,  $\text{H}_{\text{oxindole}}$ ); 7.67 (s, 1H,  $\text{H}_{\text{vinyl}}$ ); 7.94 (d, 2H,  $\text{H}_{\text{benzyl}}$ ); 8.34 (d, 2H,  $\text{H}_{\text{benzyl}}$ ); 10.71 (s, 1H, NH); ESI-MS (ES+):  $m/z = 289$  (M+Na).

### 2.2.7. 3-[4'-Dimethylaminobenzylidene]indoline-2-one 12

The synthesis was carried out with 266 mg (2 mmol) oxindole and 358 mg (2.4 mmol) of 4-dimethylaminobenzaldehyde following the procedure in 2.2.1., the product was collected by filtration and washed with ethyl acetate/petrol ether = 1:1. Yield: 504 mg brown crystals (95%), mp: 225–232 °C;  $^1\text{H}$  NMR ( $\delta$ , ppm, DMSO- $d_6$ ): 3.03 (s, 6H,  $2 \times \text{CH}_3$ ); 6.77 (m, 3H,  $\text{H}_{\text{benzyl}}/\text{H}_{\text{oxindole}}$ ); 6.93 (t, 1H,  $\text{H}_{\text{oxindole}}$ ); 7.11 (t, 1H,  $\text{H}_{\text{oxindole}}$ ); 7.60 (d, 1H,  $\text{H}_{\text{oxindole}}$ ); 7.63 (s, 1H,  $\text{H}_{\text{vinyl}}$ ); 8.43 (d, 2H,  $\text{H}_{\text{benzyl}}$ ), 10.45 (s, 1H, NH); ESI-MS (ES+):  $m/z = 287$  (M+Na).

### 2.2.8. 3-[4'-Trimethylammoniumbenzylidene]indoline-2-one-trifluoromethanesulfonate 13

Two hundred and sixty four milligrams (1 mmol) of **12** were dissolved in 10 mL of dichloromethane and 131  $\mu\text{L}$  (1.2 mmol) of ethyl-trifluoromethanesulfonate were added at rt. After stirring for 24 h the precipitate was collected by filtration and washed with ethyl acetate/petrol ether 1:1. Yield: 392 mg yellow crystals (92%); mp: 218–223 °C,  $^1\text{H}$  NMR ( $\delta$ , ppm, DMSO- $d_6$ ): 3.63 (s, 9H,  $\text{CH}_3$ ); 6.83 (d, 1H,  $\text{H}_{\text{oxindole}}$ ); 7.01 (t, 1H,  $\text{H}_{\text{oxindole}}$ ); 7.25 (t, 1H,  $\text{H}_{\text{oxindole}}$ ); 7.71 (s, 1H,  $\text{H}_{\text{oxindole}}$ ); 7.88 (s, 1H,  $\text{H}_{\text{vinyl}}$ ), 8.03 (d, 2H,  $\text{H}_{\text{benzyl}}$ ); 8.50 (d, 2H,  $\text{H}_{\text{benzyl}}$ ); 10.69 (s, 1H, NH); ESI-MS (ES+):  $m/z = 279$  (M+).

## 2.3. Radiochemical synthesis

### 2.3.1. Labelling experiments with [ $^{18}\text{F}$ ]fluoride

No-carrier-added aqueous [ $^{18}\text{F}$ ]fluoride ion was produced in a IBA CYCLONE 18/9 cyclotron by irradiation of [ $^{18}\text{O}$ ]H $_2$ O via the  $^{18}\text{O}(\text{p},\text{n})^{18}\text{F}$  nuclear reaction. The aqueous [ $^{18}\text{F}$ ]fluoride (300–500 MBq) was fixed on an anion exchange cartridge (QMA plus, Waters) and resolubilized by a solution of Kryptofix<sup>®</sup> 222 and K $_2$ CO $_3$  in a conical vial. Removal of water was accomplished by azeotropic distillation with acetonitrile in a stream of nitrogen. Finally the dried [ $^{18}\text{F}$ ]KF was dissolved in an appropriate volume of anhydrous solvent (acetonitrile, DMF, DMSO) and heated in a sealed vial in presence of 7–15 mg of the appropriate precursors **5**, **6**, **11** or **13** in an oil bath for 20 min at the indicated temperatures. After cooling the mixture was diluted with 2 mL of water and the products were monitored by radio-TLC (silicagel on aluminium, ethyl acetate/petrol ether 1:1) and analytical radio-HPLC (RP18 column, acetonitrile/water = 40:60).

### 2.3.2. Radiosynthesis of 3-[4'- $^{18}\text{F}$ ]fluorobenzylidene]indolin-2-one 14 via Knoevenagel condensation

Synthesis of 4-[ $^{18}\text{F}$ ]fluorobenzaldehyde was performed by reacting [ $^{18}\text{F}$ ]fluoride with 4-trimethylammoniumbenzaldehyde triflate<sup>22</sup> in an automated synthesizer module. Briefly 15 mg precursor dissolved in 1.0 mL of acetonitrile were heated with dried [ $^{18}\text{F}$ ]KF at 90 °C for 10 min. After cooling 11 mL of water was added and the mixture conducted on a pre-conditioned HLB-plus car-

tridge (250 mg, Waters). The cartridge was dried in a stream of nitrogen for 5 min and the 4-[ $^{18}\text{F}$ ]fluorobenzaldehyde was recovered by eluting the cartridge with 3.0 mL of ethanol. The eluent solution was directed in a separate reacting vial containing 10 mg of oxindole and 30  $\mu\text{L}$  of base. The sealed vial was heated at 90 °C for performing Knoevenagel condensation, after 20 min the mixture was cooled and conducted to semi-preparative HPLC; by using an isocratic eluent (water/acetonitrile = 1:1). The radiotracer **14** was eluted between 20 and 22 min at a flow rate of 8 mL/min. The product **14** was separated from the eluent by means of solid phase extraction (Lichrolut RP18, 500 mg, Merck), removed from the cartridge with 0.7 mL of ethanol and formulated for biological investigation with 6.5 mL of 0.9% sodium chloride solution. In this way the radiotracer **14** was synthesized in 90 min synthesis time in 4% total decay corrected yield from [ $^{18}\text{F}$ ]fluoride in radiochemical purity of 98% and a specific activity of 48–61 GBq/ $\mu\text{mol}$ .

## 2.4. Distribution coefficient

The octanol/buffer distribution coefficient ( $\log D_{\text{Oct } 7.4}$ ) at pH 7.4 was measured using radiolabelled **14** in phosphate buffer (0.1 M) and an equal volume of water-saturated *n*-octanol in separation funnel. After vortexing for 1 min, the mixture was fixed, and the two phases were allowed to separate. Aliquots of the separated phases were assayed for tracer activity by the gamma well counter. Samples were analyzed in duplicate and re-extracted three times to ensure stability of the  $\log D_{\text{Oct } 7.4}$  value.

## 2.5. Stability studies in vitro

The in vitro stability of radiotracer **14** was evaluated by radio-HPLC analysis at several time points after incubation with samples of blood and plasma. Briefly 0.5 MBq of radiotracer have been added to 400  $\mu\text{L}$  of blood sample taken from Wistar rats and incubated in a thermo-mixer at 37 °C at 600 rpm for 5, 30 and 60 min. Plasma was separated by centrifugation (3 min, 13,000g) followed by precipitation of plasma proteins with acetonitrile/water/trifluoroacetic acid (50:45:5) in a 1:2 ratio. The clear supernatant separated by second centrifugation (3 min, 13,000g) was used for analysis. For in vitro stability in rat plasma the blood cells have been removed by centrifugation before radiotracer addition and incubation.

Wistar-Unilever rats were anesthetized with Desflurane (7.0–12.0% v/v). The guide value for breathing frequency was 65 breaths/min. Animals were put in the supine position and placed on a heating pad to maintain body temperature. The spontaneous breathing rats were heparinized with 100 units/kg heparin (Heparin-Natrium 25,000-ratiopharm<sup>®</sup>, ratiopharm GmbH, Germany) by a subcutaneous injection to prevent blood clotting on intravascular catheters. After local anaesthesia by injection of Lignocain 1% (Xylocitin<sup>®</sup> loc, mibe, Jena, Germany) into the right groin, catheters were introduced into the left *arteria carotis* (0.8 mm Umbilical Vessel Catheter, Tyco Healthcare, Tullamore, Ireland) for arterial blood sampling, and a second catheter into the left *vena jugularis* vein was used for radiotracer injection. For stability studies in vivo the radiotracer **14** was injected intravenously into male Wistar rats (30 MBq) and arterial blood samples were taken 1, 3, 5, 10, 20, 30 and 60 min after injection. Plasma was separated by centrifugation followed by precipitation and removal of plasma proteins as above described.

The radio-HPLC system (Agilent 1100 series) applied for metabolite analysis was equipped with UV detection (254 nm) and an external radiochemical detector (Canberra-Packard, Radiomatic Flo-one Beta 150TR). Analysis was performed on a ZorbaxIII 300 SB-C18 (250  $\times$  9.4 mm; 5  $\mu\text{m}$ ) column with an eluent system C (water + 0.05%TFA) and D (acetonitrile + 0.04%TFA) in a gradient

15 min 50%D to 90%D and 5 min at 90%D at a flow rate of 2 mL/min.

## 2.6. Biodistribution studies in Wistar rats

The animal research committee of the Regierungspräsidium Dresden approved the animal facilities and the experiments according to institutional guidelines and the German animal welfare regulations. The experimental procedure used conforms to the *European Convention for the Protection of Vertebrate Animals used for Experimental and other Scientific Purposes* (ETS No. 123), to the *Deutsches Tierschutzgesetz*, and to the *Guide for the Care and Use of Laboratory Animals* published by the US National Institutes of Health (DHEW Publication No. (NIH) 82-23, Revised 1996, Office of Science and Health Reports, DRR/NIH, Bethesda, MD 20205). The Wistar rats (Wistar Unilever, HsdCpb: Wu, Harlan Winkelmann GmbH, Borcheln, Germany,  $138 \pm 16$  g body weight) were housed under standard conditions with free access to standard food and tap water. The biodistribution of **14** was studied in 5 male rats at 5 min and 60 min after tracer injection. The animals were anesthetized with Desflurane (Suprane, Baxter Healthcare Corporation Deerfield, IL, USA) (7.0–10.0% v/v in 30% oxygen) and 1.7 MBq **14** aliquots were administered in 500  $\mu$ L electrolyte solution E153 (Serumwerk Bernburg AG, Bernburg, Germany) with 10% ethanol and into a tail vein. After recovery from anaesthesia rats were again anaesthetized at 5 or 60 min after tracer injection, respectively. Blood was withdrawn by heart puncture, and the animals were euthanized. Organs and tissues were removed, dried, weighted, and the radioactivity was measured in a cross calibrated well counter (WIZARD, Automatic Gamma Counter, Perkin Elmer, Waltham, Ma, USA) or activimeter (Activimeter Isomed 2000; MCD Nuklear Medizintechnik, Dresden, Germany). The data were decay corrected and normalized to the amount of injected activity calculated from the activity of injection syringes before and after injection and expressed as percentage of injected activity (%ID) or standardized uptake values in biodistribution studies ( $SUV_{bio}$ ,  $SUV_{bio} = (\text{tissue activity}/\text{tissue weight})/(\text{total given activity}/\text{rat body weight})$ ). Values are quoted as mean  $\pm$  standard deviation (mean  $\pm$  SD) for a group of animals.

## 2.7. Small animal PET studies on rats and mice with xenografted FaDu tumours

Positron emission tomography experiments were performed on a established human tumour cell lines HT-29 (ECACC 91072201), a colorectal adenocarcinoma cell line and a hypopharyngeal squamous cell carcinoma line (FaDu), kept in high passage by the American Type Culture Collection ATCC HTB-43 (Rockville, MD). In nude mice, FaDu grows as a poorly differentiated, nonkeratinizing carcinoma. Following a standardized protocol, small tumour chunks were transplanted sc into the right hind leg of the recipient mice. When the tumours reached a diameter of about of 7–9 mm, imaging studies were performed. The animals were anesthetized through inhalation of Desflurane (7–10% Suprane) in 30% oxygen/air (gas flow, 1 L/min). Mice were positioned and immobilized prone with their medial axis parallel to the axial axis of the scanner and their thorax, abdomen, and hind legs (organs of interest: liver and tumour) in the centre of the field of view of the microPET<sup>®</sup> P4 (Siemens preclinical solutions, Knoxville, TN, USA) scanner. For attenuation correction, a 10 min transmission scan was obtained using a rotating <sup>57</sup>Co point source before tracer injection and collection of the emission scans. The radioactivity of the injection solution in 1 mL syringe was measured in the well counter cross-calibrated with the scanner. The emission scan of 60-min PET acquisition was started and with a delay of 30 s the infusion of the radiotracer was initiated. A solution of 0.5 mL (E153, 10% eth-

anol) of approximately 11 MBq **14** was infused over 1 min with a Harvard Apparatus 44 syringe pump (Harvard Apparatus, Holliston, Ma, USA) using a needle catheter into a tail vein. Data acquisition was performed in 3D list mode. Emission data were collected continuously. The list mode data were sorted into sinograms with 32 frames ( $15 \times 10$  s,  $5 \times 30$  s,  $5 \times 60$  s,  $4 \times 300$  s,  $3 \times 600$  s). The data were decay, scatter and attenuation corrected. The frames were reconstructed by a Ordered Subset Expectation Maximization applied to 3D sinograms (OSEM3D) with 14 subsets, 15 OSEM3D iterations, 25 maximum a posteriori (MAP) iterations, and 1.8 mm resolution using the FastMAP algorithm. The pixel size was 0.07 by 0.07 by 0.12 cm, and the resolution in the centre of field of view was 1.8 mm. No correction for partial volume effects was applied. The image volume data were converted to Siemens ECAT7 format for further processing. The image files were then processed using the ROVER software (ABX GmbH, Radeberg, Germany). Masks for defining three-dimensional regions of interest (ROI) were set and the ROI's were defined by thresholding and ROI time activity curves (TAC) were for the subsequent data analysis. The ROI data and TAC were further analyzed using R (R is available as Free Software under the terms of the Free Software Foundation's GNU General Public License in source code form) and especially developed program packages (Jörg van den Hoff, Forschungszentrum Dresden-Rossendorf, Dresden, Germany). The standardized uptake values ( $SUV_{PET}$ ,  $SUV_{PET} = (\text{activity}/\text{mL tissue})/(\text{injected activity}/\text{body weight}, \text{mL/g})$ ) were calculated in ROI.

## 3. Results and discussion

### 3.1. Synthesis of labelling precursors and reference compounds

The fluorinated non-radioactive reference compound **2** was easily obtained by the reaction of commercially available 5-fluoro-oxindole **1** with 3,5-dimethylpyrrol-2-carbaldehyde and piperidine as the base in ethanol under reflux. This special type of aldol condensation is also referred to as Knoevenagel reaction (Fig. 2).

The introduction of the isotope <sup>18</sup>F into the aromatic core may be usually accomplished via nucleophilic substitution of a nitro or trimethylammonium leaving group with [<sup>18</sup>F]fluoride in aprotic solvents.<sup>23</sup> For precursor synthesis it seems to be reasonable at first introducing the leaving group to the oxindole and completing the precursor by Knoevenagel condensation with the aldehyde in a second step (Fig. 2). In this straightforward way the nitro-precursor **5** was obtained from the corresponding 5-nitro-oxindole **3** in 72% yield.<sup>20</sup> Introduction of the *N,N*-dimethylamino group to the oxindole was achieved by electrophilic aromatic substitution with *N*-chloro-dimethylamine, a reaction that provided 5-dimethylamino-oxindole **4** in high yield of 92%.<sup>21</sup> Compound **4** has been reacted with the aldehyde to the dimethylamino-compound **6**, after subsequent quaternization with ethyl-trifluoromethanesulfonate the corresponding trimethylammonium-precursor **7** was obtained.

For developing an alternative approach for labelling the lead drug SU5416 with <sup>18</sup>F we chose the 4-position of the 3,5-dimethylpyrrol-2-carbaldehyde and synthesized a congruent nitro-precursor **15** starting from the nitro-substituted pyrrole<sup>20</sup> (Fig. 3). However all efforts of substitution with a nucleophile especially with [<sup>18</sup>F]fluoride to get the <sup>18</sup>F-labelled SU5416 derivative **16** failed due to the electron rich character of the five-membered heterocycle.

To overcome this drawback we decided replacing the pyrrole by a phenyl ring, where a labelling in *para*-position with <sup>18</sup>F should be more facilitated. This strategy was forced by the fact that for 4-fluorophenyl-substituted oxindole **10** (SU5205) was found an inhibition of ligand-induced endothelial mitogenesis for VEGF an IC<sub>50</sub> value of 5.1  $\mu$ M, what is by factor 7 higher than that for SU5416

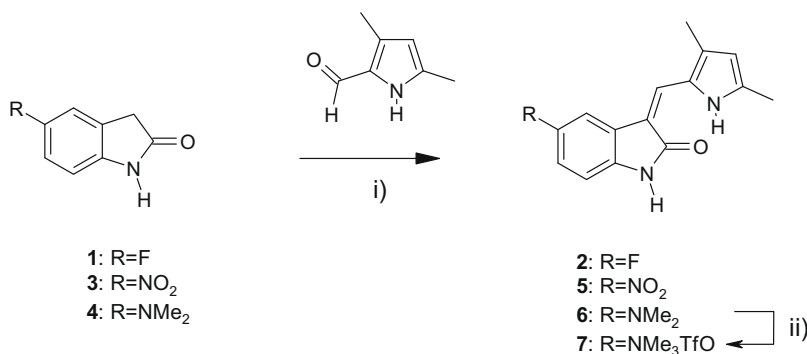


**Figure 2.** Synthesis of reference compound and precursors for labelling of SU5416, (i) EtOH, piperidine, reflux; (ii) CF<sub>3</sub>SO<sub>3</sub>CH<sub>3</sub>, CH<sub>2</sub>Cl<sub>2</sub>, rt.

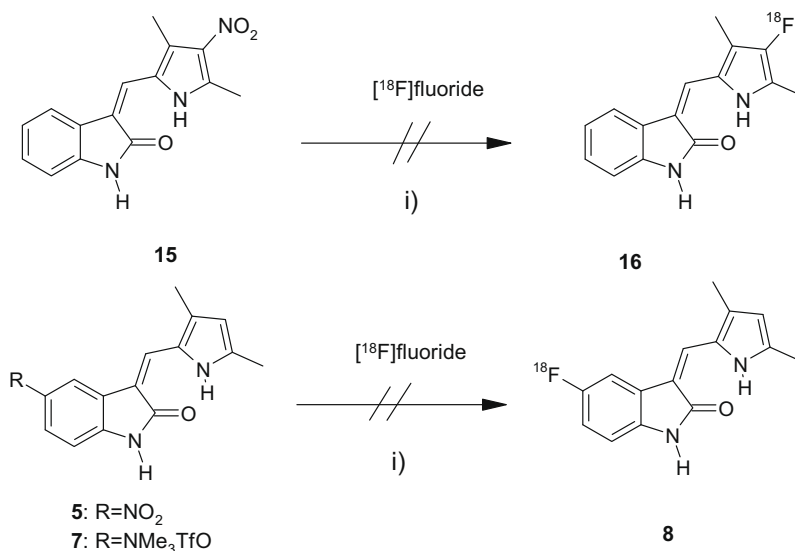


**Figure 3.** Routes for labelling of SU5416 with [<sup>18</sup>F]fluoride on the oxindole and pyrrole core, (i) Kryptofix<sub>222</sub>, DMF, acetonitrile, DMSO.

(IC<sub>50</sub> < 0.8 μM) determined with the same assay.<sup>24</sup> It was expected that this modification will result a slight drop in tyrosine kinase inhibition activity, however we proceeded on the assumption that a radiolabelled 4-[<sup>18</sup>F]fluorophenyl-substituted oxindole **10** could have adequate properties for imaging processes related with VEGFR. Table 1 displays the experimental results of in vitro RTK assays for SU5416 and **10** (SU5205) as found in literature.<sup>24</sup>

Compound **10** (SU5205) was easily prepared from oxindole **9** and 4-fluorobenzaldehyde by Knoevenagel condensation (Fig. 4). As corresponding labelling precursors the 4-nitro-phenyl substituted oxindole **11** and a 4-trimethylammonium substituted derivative **13** have been synthesized from **9** and 4-nitro-benzaldehyde and 4-dimethylaminobenzaldehyde, respectively, as depicted in Figure 4.

### 3.2. Labelling experiments with [<sup>18</sup>F]fluoride

A large scale of labelling experiments with the precursors **5** and **7** was set up by heating 7.5–15 mg of precursor with the dried [<sup>18</sup>F]KF/Kryptofix<sub>222</sub> complex in solvent volumes of 0.5–1.0 mL

**Table 1**  
Inhibition activity towards particular RTKs and inhibition of ligand-induced endothelial cell mitogenesis of SU5416 and compound **10** (SU5205)<sup>24</sup>

	FLK-1, IC <sub>50</sub> (μM)	VEGF, IC <sub>50</sub> (μM)
SU5416	0.11	<0.8
<b>10</b> (SU5205)	9.6	5.1

of acetonitrile, DMF or DMSO at temperatures in the range between 80 and 140 °C. Each reaction was examined after 20 min by radio-TLC and analytical HPLC for radiolabelled products. The non-radioactive compound **2** served as reference for UV detection by HPLC and TLC. Summarizing all of the labelling attempts it must be realized that in no cases the desired radiotracer **8** has been formed. In a row of experiments using trimethylammonium-precursor **7** and acetonitrile as solvent, a new radiolabelled product was detected in up to 12% yield, but its retention time on HPLC was dissenting with that from the standard **2**. The structure of this from its elution profile on HPLC more hydrophilic radiolabelled product could not be identified. This findings were much more disappointing because the successful radiolabelling of another 5-nitro-substituted oxindole (SU11248) with [<sup>18</sup>F]fluoride was recently described.<sup>19</sup>

To use an alternative labelling position besides the oxindole ring and after unsuccessful efforts of labelling a 3-nitro-substituted pyrrol precursor<sup>20</sup> with [<sup>18</sup>F]fluoride we concentrated on the phenyl-substituted oxindole derivative **10** (SU5205) as surrogate for SU 5416. For labelling 5–10 mg of precursors **11** and **13**, respectively, were heated with dried [<sup>18</sup>F]KF/Kryptofix<sub>222</sub> at various temperatures and reaction times. The results of the labelling experiments are shown in Table 2, the yield of the radiolabelled product **14** was quantified by gamma detection on analytical HPLC, the retention time of UV-absorption of the non-radioactive compound **10** served as reference.

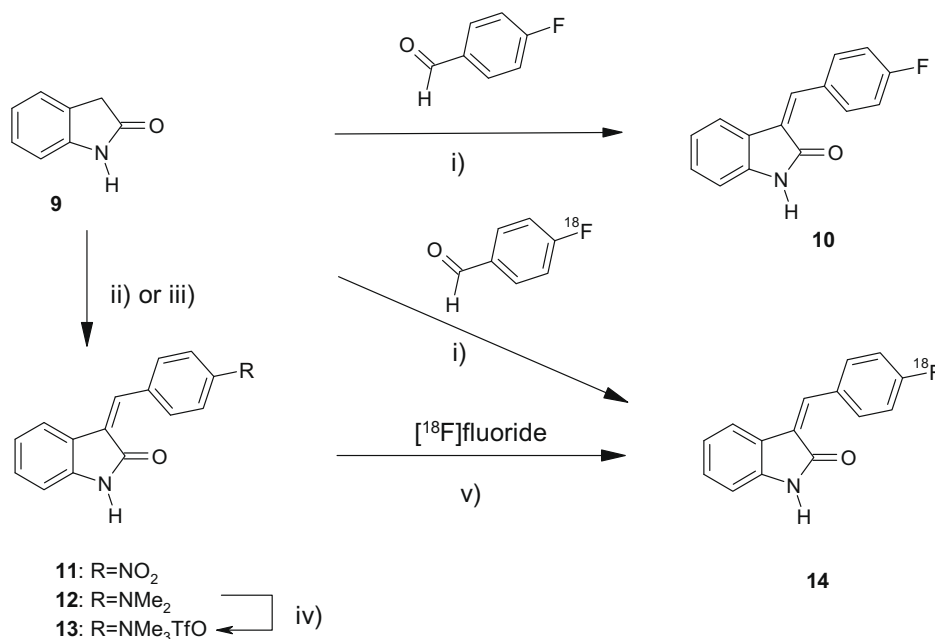


**Figure 4.** Synthesis of precursors and reference compounds and radiosynthesis of 3-[4-[<sup>18</sup>F]fluorobenzylidene]indolin-2-one **14**, (i) EtOH, piperidine, reflux; (ii) 4-nitrobenzaldehyde, EtOH, piperidine, reflux; (iii) 4-dimethylamino-benzaldehyde, EtOH, reflux; (iv) CF<sub>3</sub>SO<sub>3</sub>CH<sub>3</sub>, CH<sub>2</sub>Cl<sub>2</sub>, rt; (v) Kryptofix<sub>222</sub>, K<sub>2</sub>CO<sub>3</sub>, DMF, acetonitrile.

**Table 2**

Yields and conditions of radiosynthesis of 3-[4-[<sup>18</sup>F]fluorobenzylidene]indolin-2-one **14** starting from precursors **11** and **13** by radiolabelling with [<sup>18</sup>F]fluoride

Run	Precursor	Mass (mg)	Solvent	Reaction time (min)	Temperature (°C)	Yield of <b>14</b>
1	<b>11</b>	7.5	DMF	10	120	—
2	<b>11</b>	7.5	DMF	10	140	1.2
3	<b>11</b>	7.5	DMF	10	160	1.6
4	<b>13</b>	10	DMF	20	100	5.2
5	<b>13</b>	10	DMF	20	120	5.4
6	<b>13</b>	10	DMSO	20	120	1.8
7	<b>13</b>	10	CH <sub>3</sub> CN	20	80	2.6
8	<b>13</b>	10	CH <sub>3</sub> CN	20	100	8.4
9	<b>13</b>	10	CH <sub>3</sub> CN	20	120	6.4
10	<b>13</b>	10	CH <sub>3</sub> CN	10	100	5.0
11	<b>13</b>	10	CH <sub>3</sub> CN	40	100	4.0
12	<b>13</b>	5.0	CH <sub>3</sub> CN	20	100	0.6

By interpretation of the results in Table 2 it becomes clear visible, that the nitro-substituted precursor **11** gave only poor yield of 1.6% in labelling with [<sup>18</sup>F]fluoride, even at high temperatures of 160 °C (runs 1–3). The trimethylammonium-substituted precursor **13** showed under standard conditions in DMSO and DMF also low but in relation to **11** increased yields up to 5.4%. The solvent of choice for labelling precursor **13** was found to be acetonitrile whereby a distinct dependence of labelling yield from the reaction temperature was determined. The optimum reaction temperature was found to be 100 °C, where a maximum yield of 8.4% was achieved (runs 7–9). Bisection or doubling of reaction time did not give an improvement (runs 10 and 11), as well as decline of precursor amount to 5 mg gave only 0.6% product (run 12).

### 3.3. Labelling experiments with 4-[<sup>18</sup>F]fluorobenzaldehyde by Knoevenagel condensation

We found the labelling yield of 8.4% for **14** starting from precursor **13** in general dissatisfying compared with the radiosynthesis of 4-[<sup>18</sup>F]fluorobenzaldehyde where starting with a 4-trimethylammonium-benzaldehyde trifluoromethanesulfonate precursor labelling yields up to 80% could be achieved.<sup>22,25</sup>

From this background was decided to enter an alternative synthetic route covering the synthesis of 4-[<sup>18</sup>F]fluorobenzaldehyde as labelling block and performing a Knoevenagel condensation with oxindole in an additional step. This approach was described earlier for the synthesis of [<sup>18</sup>F]fluorophenylalanine by reaction of 4-[<sup>18</sup>F]fluorobenzaldehyde with 2-phenyl-5-oxazolone.<sup>26</sup> A prerequisite for this pre-labelling method is the availability of 4-[<sup>18</sup>F]fluorobenzaldehyde what is produced in most published synthetic procedures with DMSO as solvent.<sup>22,25,26</sup> However we found by HPLC investigation the chemical and radiochemical purity of 4-[<sup>18</sup>F]fluorobenzaldehyde not sufficient for further reaction. In contrast when heating 4-trimethylammonium-benzaldehyde trifluoromethanesulfonate in acetonitrile at 90 °C and separating the product via solid phase extraction, after elution with ethanol 4-[<sup>18</sup>F]fluorobenzaldehyde with radiochemical purity >91% was obtained containing only traces of non-radioactive by-products. For solid phase extraction HLB-plus cartridges (Waters) turned out to be the most appropriate compared to other commercial RP18 SPE-cartridges. After washing the cartridge with water for removal of [<sup>18</sup>F]fluoride and residual precursor the 4-[<sup>18</sup>F]fluorobenzaldehyde was recovered by elution with 3 mL of ethanol and conducted to a second reacting vessel, containing the oxindole **9** and

a base. For optimization of the Knoevenagel condensation with 4-[<sup>18</sup>F]fluorobenzaldehyde a number of bases under distinct reaction conditions has been tested, the results are presented in Table 3.

In Table 3 the bases used are arranged with increasing pK<sub>a</sub> and it seems that basicity has an influence on the progress of reaction. Best results could be obtained by using amine bases piperidine (18–29%) or diethylamine (48%). Application of stronger amine bases (DABCO, *N*-ethyl-diisopropyl amine) or weaker bases (ammonium acetate, 2,6-di-*tert*-butyl pyridine) resulted in lower or no product formation. Phosphazane as very strong base yielded 26% of desired product **14** along with formation of large amounts of non-identified side products. Additional there seems to be an optimum in the amount of oxindole **9** used, so by starting with 5 mg only 8% yield was obtained, utilization of 10 mg raised the yield to 18%, but further improvement with 15 mg of **9** was not achieved (runs 4–6).

By increasing the reaction temperature to 100 °C an enhanced yield of 29% was obtained, on the other hand this resulted in a very high pressure in the reactor together with uncontrolled release of the solvent ethanol (run 7). The similar high yield of 28% of **14** could be achieved by utilization of 50 μL of piperidine at 90 °C but in this case more than 30% of radioactive by-products were observed what turned out as not feasible (run 8). In addition we

found out that a prolongation of the reaction time to 40 min did not result in an insignificant improvement of yield (run 9). Finally we ascertained that the Knoevenagel condensation of oxindole and 4-[<sup>18</sup>F]fluorobenzaldehyde with diethylamine was the best choice (48% yield) and was selected it for all further labelling experiments (run 3).

### 3.4. Biodistribution

The distribution of radioactivity in selected tissues and organs was studied in normal Wistar rats at different time points (1, 5, 10, 30 and 60 min) after injection of 3-[4'-[<sup>18</sup>F]fluorobenzylidene]indolin-2-one **14**. The results are depicted in Table 4 (SUV<sub>Biodis</sub>) and Table 5 (%ID).

The radiotracer was rapidly cleared from the blood with a starting radioactivity concentration (SUV<sub>Biodis</sub>) of 0.83 ± 0.16 reaching 0.15 ± 0.02 at 60 min p.i. The adipose tissue was the only organ, which remained the activity (1.15 ± 0.25 (60 min)) after a fast uptake (0.70 ± 0.02 (1 min)). The organs with the highest starting activity concentration such as adrenals, lung, kidneys, liver, brain, heart and pancreas (4.95 ± 0.80, 4.26 ± 0.41, 3.36 ± 0.16, 2.98 ± 0.46, 2.84 ± 0.15, 2.51 ± 0.05, 2.40 ± 0.26) show over 60 min a clearance. The slowest clearance was observed in the

**Table 3**  
Yields and conditions of radiosynthesis of 3-[4'-[<sup>18</sup>F]fluorobenzylidene]indolin-2-one **14** via Knoevenagel condensation of 4-[<sup>18</sup>F]fluorobenzaldehyde with oxindole

Run	Mass of oxindole (mg)	Time (min)	Base	pK <sub>a</sub>	Temperature (°C)	Yield of <b>14</b> (%)
1	10	20	CH <sub>3</sub> COONH <sub>4</sub> <sup>a</sup>	2.3	90	–
2	10	20	2,6-Di- <i>t</i> -butyl-pyridine <sup>b</sup>	3.6	90	14
3	10	20	Diethylamine <sup>b</sup>	10	90	48
4	5.0	20	Piperidine <sup>b</sup>	11	90	8
5	10	20	Piperidine <sup>b</sup>	11	90	18
6	15	20	Piperidine <sup>b</sup>	11	90	19
7	10	20	Piperidine <sup>b</sup>	11	100	29
8	10	20	Piperidine <sup>c</sup>	11	90	28 <sup>e</sup>
9	10	40	Piperidine <sup>b</sup>	11	90	26
10	10	20	<i>N</i> -Ethyl-diisopropyl-amine <sup>b</sup>	12	90	7
11	10	20	DABCO <sup>d</sup>	18	90	3
12	10	20	Phosphazane-base <sup>b</sup>	40	90	26 <sup>e</sup>

<sup>a</sup> 25 mg.

<sup>b</sup> 30 μL.

<sup>c</sup> 50 μL.

<sup>d</sup> 10 mg.

<sup>e</sup> >30% of radiolabelled by-products

**Table 4**  
Radioactivity concentration in rat organs and tissues after single intravenous application of **14** as mean ± SD as SUV<sub>Biodis</sub>

Time p.i. (min)	1 min			5 min			10 min			30 min			60 min		
	Mean	SD	<i>n</i>	Mean	SD	<i>n</i>	Mean	SD	<i>n</i>	Mean	SD	<i>n</i>	Mean	SD	<i>n</i>
Blood	0.83	0.16	2	0.56	0.04	6	0.47	0.03	2	0.27	0.02	2	0.15	0.02	6
Brown adipose tissue	1.42	0.40	2	2.29	0.39	6	1.83	0.33	2	0.98	0.32	2	0.63	0.10	6
Hair and skin	0.67	0.03	2	0.92	0.12	6	0.74	0.12	2	0.48	0.02	2	0.19	0.03	6
Brain	2.84	0.15	2	1.67	0.15	6	0.97	0.13	2	0.41	0.09	2	0.18	0.04	6
Pancreas	2.40	0.26	2	1.66	0.12	6	1.13	0.16	2	0.55	0.11	2	0.30	0.07	6
Spleen	0.98	0.07	2	0.79	0.06	6	0.52	0.01	2	0.28	0.05	2	0.13	0.03	6
Adrenals	4.95	0.80	2	5.71	1.55	6	3.20	0.31	2	1.39	0.42	2	1.11	0.39	6
Kidney	3.36	0.16	2	2.64	0.28	6	2.27	0.21	2	1.69	0.20	2	0.97	0.07	6
Adipose tissue	0.70	0.02	2	1.21	0.28	6	1.26	0.05	2	1.17	0.07	2	1.15	0.25	6
Muscle	0.82	0.34	2	0.83	0.05	6	0.69	0.05	2	0.45	0.11	2	0.19	0.03	6
Heart	2.52	0.05	2	1.33	0.10	6	0.88	0.00	2	0.44	0.09	2	0.20	0.04	6
Lung	4.26	0.41	2	1.30	0.08	6	0.85	0.07	2	0.47	0.10	2	0.27	0.04	6
Thymus	1.10	0.07	2	0.82	0.10	6	0.53	0.04	2	0.26	0.04	2	0.13	0.02	6
Thyroid	1.55	0.21	2	0.99	0.09	6	0.75	0.10	2	0.40	0.14	2	0.16	0.02	6
Harderian glands	1.92	0.23	2	2.43	0.28	6	1.91	0.33	2	1.07	0.22	2	0.46	0.09	6
Liver	2.98	0.46	2	3.74	0.27	6	3.03	0.20	2	1.68	0.42	2	1.30	0.11	6
Femur	0.89	0.16	2	0.64	0.07	6	0.51	0.01	2	0.28	0.02	2	0.19	0.01	6
Testes	0.00	0.00	2	0.41	0.32	6	0.00	0.00	2	0.00	0.00	2	0.19	0.01	6

**Table 5**  
Radioactivity amount in rat organs after single intravenous application of **14** as mean  $\pm$  SD as %ID

Time p.i. (min)	1 min			5 min			10 min			30 min			60 min		
	mean	SD	n	mean	SD	n	mean	SD	n	mean	SD	n	mean	SD	n
Brain	3.09	0.27	2	1.87	0.32	6	1.09	0.16	2	0.44	0.06	2	0.20	0.05	6
Pancreas	0.56	0.03	2	0.38	0.03	6	0.28	0.10	2	0.11	0.02	2	0.07	0.01	6
Spleen	0.31	0.00	2	0.23	0.04	6	0.14	0.01	2	0.08	0.01	2	0.04	0.02	6
Adrenals	0.15	0.01	2	0.17	0.06	6	0.10	0.00	2	0.04	0.00	2	0.04	0.02	6
Kidney	3.13	0.11	2	2.51	0.42	6	2.28	0.35	2	1.45	0.04	2	0.91	0.11	6
Heart	1.01	0.17	2	0.54	0.04	6	0.35	0.02	2	0.18	0.03	2	0.08	0.02	6
Lung	2.68	0.01	2	1.02	0.08	6	0.66	0.00	2	0.33	0.02	2	0.19	0.02	6
Thymus	0.50	0.20	2	0.34	0.11	6	0.23	0.03	2	0.08	0.01	2	0.05	0.01	6
Thyroid	0.09	0.01	2	0.08	0.02	6	0.05	0.02	2	0.03	0.00	2	0.01	0.00	6
Harderian glands	0.29	0.03	2	0.34	0.09	6	0.25	0.01	2	0.14	0.02	2	0.06	0.02	6
Liver	17.16	2.15	2	18.40	1.53	6	17.84	1.11	2	8.95	1.87	2	5.98	0.61	6
Femur	0.44	0.08	2	0.35	0.08	6	0.32	0.00	2	0.13	0.01	2	0.11	0.01	6
Testes	0.00	0.00	2	0.38	0.64	6	0.00	0.29	2	0.00	0.03	2	0.24	0.02	6
Intestine	8.84	0.00	2	13.96	2.27	6	0.00	0.43	2	0.00	4.63	2	30.16	2.22	6
Stomach	0.71	0.00	2	0.94	0.69	6	0.00	0.28	2	0.00	0.00	2	0.60	0.40	6
Urine calculated	3.97	2.46	2	2.39	1.14	6	6.98	0.58	2	11.23	4.39	2	43.53	5.45	6

adrenals, lung, kidney, liver, brain, heart and pancreas (% activity at 60 min in comparison to 5 min: 95, 46, 37, 35, 30, 27, 26). Organs with the highest tissue to blood ration at 5 min that extracted the activity from the blood were adrenals, liver, kidney, Harderian glands, brown adipose tissue, brain, pancreas, heart and lung (10.2, 6.7, 4.7, 4.4, 4.1, 3.0, 3.0 tissue/blood at 5 min). This situation qualitatively did not alter after 60 min, the highest tissue to blood ratios remained in liver, adipose tissue, adrenals, brown adipose tissue Harderian glands, pancreas, lung heart (8.9, 7.9, 7.6, 6.8, 4.3, 3.2, 2.1, 1.8, 1.4 tissue/blood at 60 min).

The elimination of the 3-[4'-<sup>18</sup>F]fluorobenzylidene]indolin-2-one **14** reflects in the time course of the <sup>18</sup>F-activity amount in the body (Table 5, Fig. 6). After 5 min were 18.40  $\pm$  1.53%ID and 13.96  $\pm$  2.27%ID in the intestine and liver, but only 2.51  $\pm$  0.42%ID and 2.39  $\pm$  1.14%ID in the kidneys and urine. However, after 60 min were 43.53  $\pm$  5.45%ID and 30.16  $\pm$  2.22%ID in the urine and intestine. The liver and kidneys contained at this time 5.98  $\pm$  0.61%ID and 0.91  $\pm$  0.11%ID, respectively. Activity amount in the carcass was 17.18  $\pm$  2.98%ID at 60 min.

Taken together, the dominating property of 3-[4'-<sup>18</sup>F]fluorobenzylidene]indolin-2-one **14** is the high lipophilicity with a log *D* of 3.39 determined by the shake flask technique in *n*-octanol/phosphate buffer at pH 7.4 causing that directly after injection, when the most activity in the blood was existing as the original compound (see Section 3.5) the radiotracer was fast distributed into the adipose tissue increasing from 1 to 5 min and maintained at this level over the observation time. Also a high uptake was observed in well perfused tissues like adrenals, liver, lung and brain. However, the decrease of original compound in the blood plasma shifted the equilibrium, so that the non-bound activity in the tissue was released and eliminated.

The high distribution coefficient of 3.39 did not prevent the brain uptake through the blood brain barrier even if it is known that an optimal log *P* value for BBB penetration should be 1.5–2.7.<sup>27</sup> This demonstrates that **14** is not a substrate of the multidrug resistant system. All these effects are evidences for a high extraction of the radiotracer.

The heart uptake is in ranges achieved by PET-tracers for imaging myocardial transporters like 4-[<sup>18</sup>F]fluorometaraminol,<sup>28</sup> an amino-alcohol bearing an 4-fluoro-phenyl-substituent too, but in disadvantage to 4-[<sup>18</sup>F]FMR] the radiotracer **14** displays a very high uptake of the lungs. Another question is, as a result of the low metabolic stability of **14** as discussed in Section 3.5., whether the uptake of radioactivity in brain and heart derives from the original radiotracer and not from one of its metabolites.

### 3.5. Stability investigations

The metabolism of 3-[4'-<sup>18</sup>F]fluorobenzylidene]indolin-2-one **14** was investigated in vitro by treatment in samples of blood, plasma and as well as in vivo by analyzing arterial blood plasma samples at different time points. The amount of intact component over time in plasma and in blood samples in vitro as well as in blood samples in vivo is depicted in Figure 5.

As clear visible at Figure 5 the radiotracer **14** was almost stable over 60 min in blood and in blood plasma showing 84% and 96% of original compound, respectively. In contrast, in vivo arterial blood samples indicated that the tracer with a retention time of about 11 min was metabolized rapidly into two more polar metabolites with 6 and 9 min retention time, respectively. The biliary eliminated metabolite (*t<sub>R</sub>* 5.7 min) was detected in the intestine.

Interestingly in the brain was found also one metabolite together with the original tracer, what means that both radioactive compounds have passed the blood brain barrier. In summary 1 min after radiotracer injection 70%, at 3 min 54%, at 5 min 40%, at 10 min 18% and at 20 min 12% of the intact radiotracer could be detected; 60 min past injection the original compound was practically no more present. The time course of the original compound in the plasma could be described by a two-phase elimina-

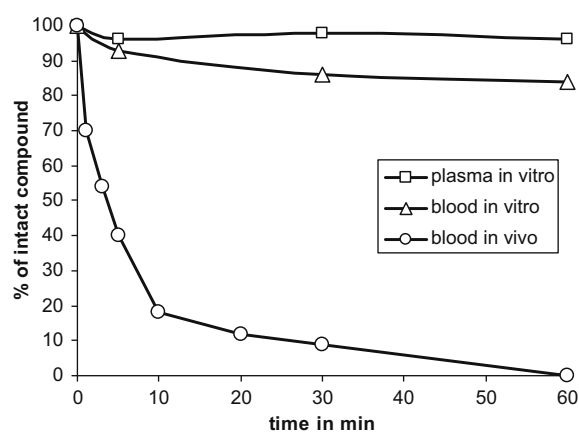


**Figure 5.** Metabolic stability of radiotracer **14** in vitro and in vivo expressed as % of total activity.

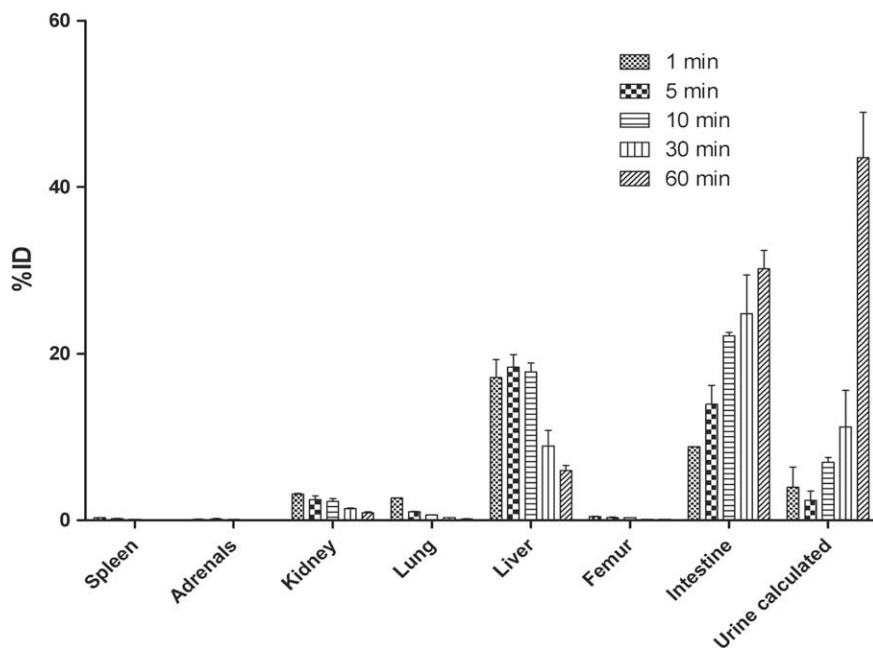


Figure 6.  $^{18}\text{F}$ -activity distributions in the excreting and eliminating organs of Wistar rats (mean  $\pm$  SD, data from Table 4).

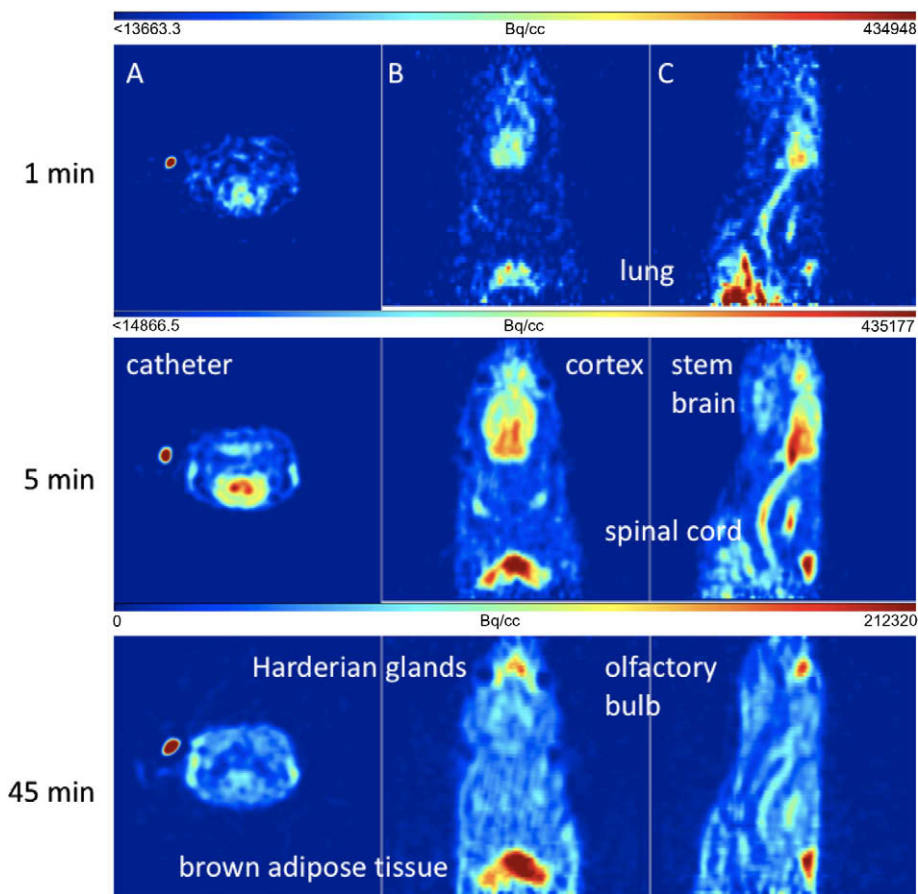


Figure 7. Transversal (A), coronal (B) and sagittal (C) sections from a PET study with **14** in a Wistar rat after 1, 5 and 45 min p.i.

tion with half lives of 8 and 267 s. These somehow surprising findings pushed us to gather more information on the structure of the metabolites and we compared the retention time with that of known reference substances. It was found that the retention time of one radio-metabolite was high conform with fluorobenzene, so

it is likely that the radiotracer **14** is transformed in vivo to [ $^{18}\text{F}$ ]fluorobenzene at least. The other metabolite at 6 min could be represent a derivative of **14** which was hydroxylated at the 5 position of the benzene ring like it was shown for the lead compound SU5416.<sup>29</sup>

### 3.6. Small animal PET studies

Small animal PET imaging with 3-[4'- $^{18}\text{F}$ ]fluorobenzylidene]indolin-2-one **14** was performed with Wistar rats, HT-29 and FaDu tumour bearing mice after single intravenous application. The results confirm the findings obtained in the biodistribution profile, showing radioactivity in brain, lung, heart and liver (Fig. 7). After 1 h radioactivity was observed in the olfactory bulb, the Harderian glands and the brown adipose tissue. The  $^{18}\text{F}$ -activity distribution in the mice was comparable (Fig. 8). However, in the tumour almost no radioactivity uptake was detected at 45 min p.i. One reason for that behaviour is certainly the resulting low area under the time–activity curve of the blood as well as the low metabolic in vivo stability of the radiotracer in mice. Figure 9 displays exemplarily the time–activity curves of **14** of the brain, blood, liver, and tumour in FaDu bearing mice, showing that the activity has been practically cleared from the large organs.

### 4. Summary and concluding remarks

The aim of the present work was the labelling of an inhibitor of tyrosine kinase with the oxindole scaffold of SU5416 with the positron emitting isotope fluorine-18. Because of the introduction of

the radionuclide into the oxindole core as well into the pyrrole core of SU5416 was unsuccessful, we developed 3-[4'-fluorobenzylidene]indolin-2-one **10** (SU5205) as surrogate for SU5416 by substitution of the dimethyl-pyrrol moiety by a 4-fluoro-phenyl ring. The radiolabelled analogue 3-[4'- $^{18}\text{F}$ ]fluorobenzylidene]indolin-2-one **14** could be prepared in a two-step procedure by Knoevenagel condensation of oxindole and 4- $^{18}\text{F}$ fluorobenzaldehyde in a remote controlled synthesizer unit, in the course of this the reaction conditions and the influence of different bases has been optimized.

The radiopharmacological investigation of the radiotracer **14** resulted in the findings that the compound, although stable in vitro is metabolized in vivo very rapidly, what means that 20 min past injection, only 12% of the original tracer could be detected in arterial blood samples. Biodistribution and PET studies showed that the radiotracer enters the brain in spite of the high lipophilicity and the heart, what is displayed in a brain uptake of 2.84% and heart uptake of 2.52% of standardized activity concentration, respectively.

The small animal PET investigations on HT-29 and FaDu tumour bearing mice did not indicate any uptake of radioactivity in the tumour what is not surprising in respect to the in vivo instability of the substance. The lack of stability and the only moderate  $\text{IC}_{50}$  affinity towards VEGF-RTKs makes compound **14** not a suitable

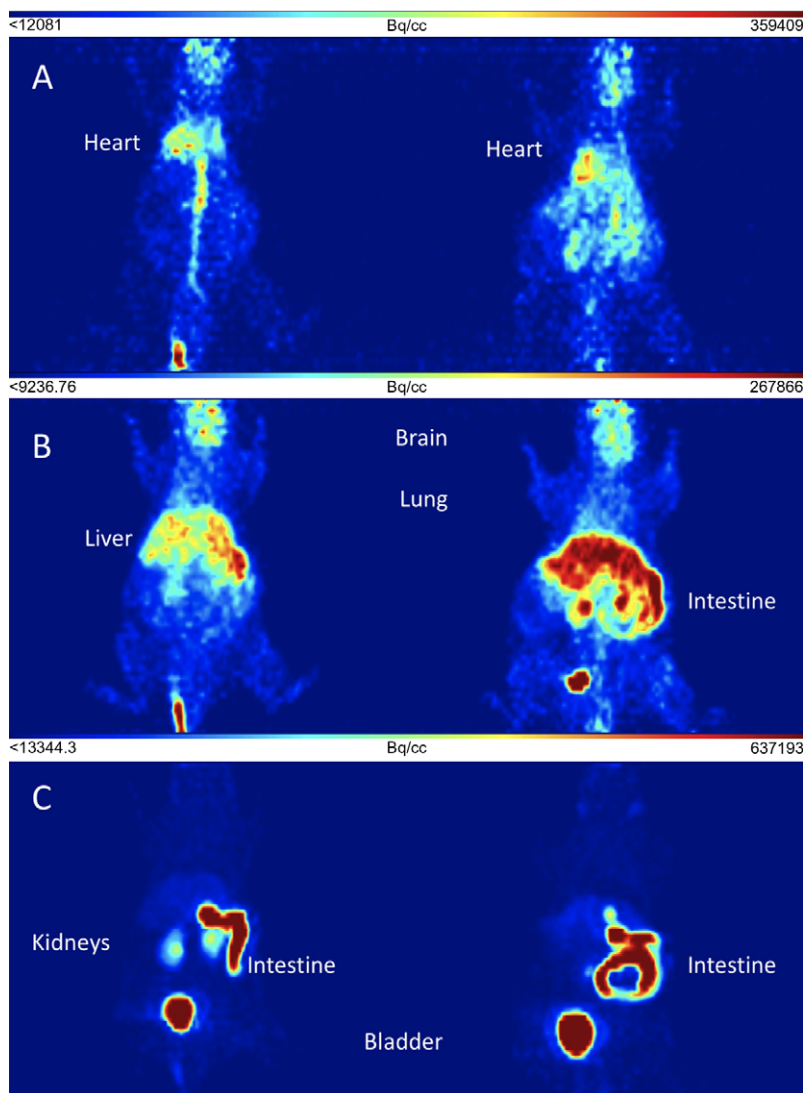


**Figure 8.** Transversal (A), coronal (B) and sagittal (C) sections from a PET study with **14** in a FaDu tumour bearing mouse after 1, 5 and 45 min p.i.

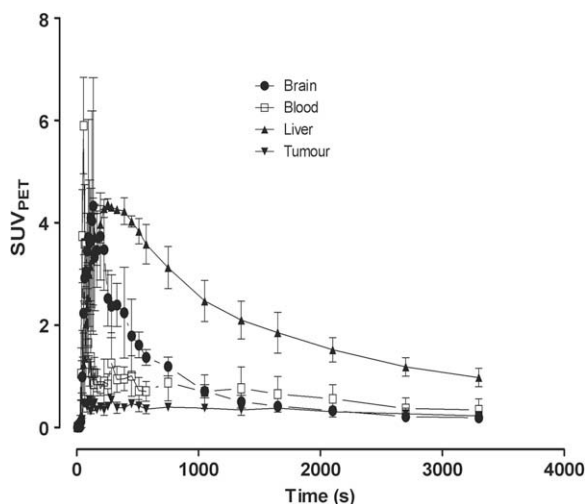


**Figure 9.** Time-activity curves from a PET study with **14** with two FaDu tumour bearing mice (mean  $\pm$  SD).

radiotracer for imaging receptor tyrosine kinases and it will need a radiolabelled derivative with sub nanomolar affinity similar to the original structure of SU5416 and SU11248 to decide if this class of compounds basing on the structure of oxindole can be used as radiotracers for monitoring angiogenic processes.

However the present study underlines that the Knoevenagel condensation with 4-[ $^{18}\text{F}$ ]fluorobenzaldehyde is a general synthesis approach for the preparation of  $^{18}\text{F}$ -labelled compounds containing a benzylidene motif.

#### Acknowledgements

The authors wish to thank Stephan Preusche for radioisotope production and Regina Herrlich and Andrea Suhr for assistance at the radiopharmacological investigations.

#### References and notes

1. Levitzki, A. *Eur. J. Cancer* **2002**, *38*, S11.

2. Rosen, L. S. *Cancer Control* **2002**, *9*, 36.
3. Arora, A.; Scholar, E. M. *J. Pharm. Exp. Ther.* **2005**, *315*, 971.
4. Zips, D.; Eicheleler, W.; Geyer, P.; Hessel, F.; Dörfler, A.; Thames, H. D.; Haberey, M.; Baumann, M. *Cancer Res.* **2005**, *65*, 5374.
5. Haubner, R.; Wester, H. J. *Curr. Pharm. Des.* **2004**, *10*, 1439.
6. Choe, Y. S.; Lee, K. H. *Curr. Pharm. Des.* **2007**, *13*, 17.
7. Holt, D. P.; Ravert, H. T.; Dannals, R. F.; Pomper, M. G. *J. Labelled Compd. Radiopharm.* **2006**, *49*, 883.
8. Wang, J. Q.; Gao, M.; Miller, K. D.; Sledge, G. W.; Zheng, Q. H. *Bioorg. Med. Chem. Lett.* **2006**, *16*, 4102.
9. Ben-David, I.; Rozen, Y.; Ortu, G.; Mishani, E. *Appl. Radiat. Isot.* **2003**, *58*, 209.
10. Mishani, E.; Abourbeh, G.; Rozen, Y.; Jacobson, O.; Laky, D.; Ben David, I.; Levitzki, A.; Shaul, M. *Nucl. Med. Biol.* **2004**, *31*, 469.
11. Fredrikson, A.; Johnström, P.; Thorell, J. O.; von Heijne, G.; Hassan, M.; Eksborg, S.; Kogner, P.; Borgström, P.; Ingvar, M.; Stone-Elander, S. *Life Sci.* **1999**, *65*, 165.
12. DeJesus, O. T.; Murali, D.; Flores, L. G.; Converse, A. K.; Dick, D. W.; Oakes, T. R.; Roberts, A. D.; Nickles, R. J. *J. Labelled Compd. Radiopharm.* **2003**, *46*, S1.
13. Dissoki, S.; Desideriu, L.; Mishani, E. *J. Labelled Compd. Radiopharm.* **2006**, *49*, 533.
14. Seimille, Y.; Phelps, M. E.; Czernin, J.; Silverman, D. H. S. *J. Labelled Compd. Radiopharm.* **2005**, *48*, 829.
15. Vasdev, N.; Dorff, P. N.; Gibbs, A. R.; Nandan, E.; Reid, L. M.; O'Neil, J. P.; VanBrocklin, H. F. *J. Labelled Compd. Radiopharm.* **2005**, *48*, 109.
16. Kil, K. E.; Ding, Y. S.; Lin, K. S.; Alexoff, D.; Kim, S. W.; Shea, C.; Xu, Y.; Muench, L.; Fowler, J. S. *Nucl. Med. Biol.* **2007**, *34*, 153.
17. Eskens, F. *Br. J. Cancer* **2004**, *90*, 1.
18. Mendel, D. B.; Laird, A. D.; Smolich, B. D.; Blake, R. A.; Liang, C.; Hannah, A. L.; Shaheen, R. M.; Ellis, L. M.; Weitman, S.; Shawver, L. K.; Cherrington, J. M. *Anti-Cancer Drug Des.* **2000**, *15*, 29.
19. Wang, J. Q.; Miller, K. D.; Sledge, G. W.; Zheng, Q. H. *Bioorg. Med. Chem. Lett.* **2005**, *15*, 4380.
20. Kniess, T.; Kuchar, M.; Wuest, F. *Synth. Commun.* **2008**, *38*, 3017.
21. Minisci, F.; Galli, R.; Cecere, M. *Chim. Ind. (Milan)* **1966**, *48*, 1324.
22. Wilson, A. A.; Dannals, R. F.; Ravert, H. T.; Wagner, H. N., Jr. *J. Labelled Compd. Radiopharm.* **1990**, *28*, 1189.
23. Coenen, H. H. Fluorine-18 Labelling Methods: Features and Possibilities of Basic Reactions. PET Chemistry—The Driving Force in Molecular Medicine. Ernst Schering Research Foundation Workshop, Springer: Berlin, Heidelberg, New York, 2007, 62, 15–50.
24. Tang, P. L.; Sun, L.; McMahon, G. US005834504A, 1998.
25. Iwata, R.; Pascali, C.; Boggi, A.; Horvath, G.; Kovacs, Z.; Yanai, K.; Ido, T. *Appl. Radiat. Isot.* **2000**, *52*, 87.
26. Lemaire, C.; Guillaume, M.; Christiaens, L.; Palmer, A. J.; Cantineau, R. *Appl. Radiat. Isot.* **1987**, *38*, 1033.
27. Pajouhesh, H.; Lenz, G. R. *NeuroRx* **2005**, *2*, 541.
28. Langner, O.; Valette, H.; Dollé, F.; Halldin, C.; Loc'h, C.; Fuseau, C.; Coulon, C.; Ottavini, M.; Bottlaender, M.; Mazière, B.; Crouzel, C. *Nucl. Med. Biol.* **2000**, *27*, 233.
29. Antonian, L.; Zhang, H.; Yang, C.; Wagner, G.; Shawver, L. K.; Shet, M.; Ogilvie, B.; Madan, A.; Parkinson, A. *Drug Metab. Dispos.* **2000**, *28*, 1505.